ARTICLE NO. 79-0012R

C80-027

Calculation of Transonic Inlet Flowfields Using Generalized Coordinates

20005
20018

Lee-tzong Chen* and D. A. Caughey†
McDonnell Douglas Corporation, St. Louis, Mo.

A method for calculating inviscid supercritical flowfields about axisymmetric inlet cowls with centerbodies is presented. A finite-difference approximation to the full-potential equation is solved under a general coordinate transformation, using a numerical evaluation of the transformation matrix at each mesh point. For the present problem, a boundary conforming coordinate system was generated by a sequence of conformal and shearing transformations, but this transformation is not essential to the method. Both the quasiconservative and nonconservative forms of Jameson's rotated differencing scheme are used, and the difference equations are solved by relaxation. Numerical results for pressure distributions generally agree well with experiment.

Introduction

SINCE the initial success of Murman and Cole[1] in applying the type-dependent differencing concept to the transonic small-disturbance equation, this technique has been extensively applied to compute transonic flowfields about airfoils, using both the small-disturbance and full-potential equations. For flowfields around blunt bodies, the full-potential equation is required to properly resolve the solution in the vicinity of the stagnation points. The introduction of the rotated differencing scheme by Jameson[2] enables the use of line relaxation for solving the full-potential equation. There have been many successful applications of the rotated difference scheme to compute inviscid transonic flowfields around blunt-nosed bodies, including nacelle inlets and wing-body configurations. For a flowfield around a nacelle inlet, Arlinger[3] applied a conformal mapping technique to transform the full-potential equation to a boundary conforming coordinate system. Caughey and Jameson[4] solved the same problem using a sequence of simpler transformations, and studied ways to accelerate the iteration scheme used to solve the difference equations. Reyhner[5,6] solved the full-potential equation in a Cartesian mesh. This requires an interpolation scheme to accurately treat the surface boundary condition. The mapping techniques generally require transforming the governing equations under the sequence of mappings. For complex geometries, these transformations can become a lengthy and tedious process. The boundary interpolation scheme has the advantage of always differencing the equation in Cartesian coordinates. There are, however, various types of irregular boundary elements, and the effort required to keep track of surface-mesh intersections is a major drawback in the application of this scheme. Caughey and Jameson[7] proposed a finite-difference scheme to compute the supercritical flowfield about wing-body configuration using a form of the quasilinear potential equation written in contravariant velocity components. Using local coordinate transformations, the need to transform the governing equation under the required sequence of mapping is avoided, while the accuracy and topological simplicity of the transformation method is retained. In the overlapping element formulation they suggested, only first derivatives of the potential function are calculated in each mesh element. By suitable differencing of quantities in neighboring elements, they compute the second derivatives required in the potential equation. In the present work, a more direct approach is proposed using a second-order, nine-point element, where the potential derivatives are continuous up to the second order. Derivatives in the physical and computational planes are related through the application of a second-order shape function; therefore, the governing potential equation written in Cartesian coordinates can be applied directly.

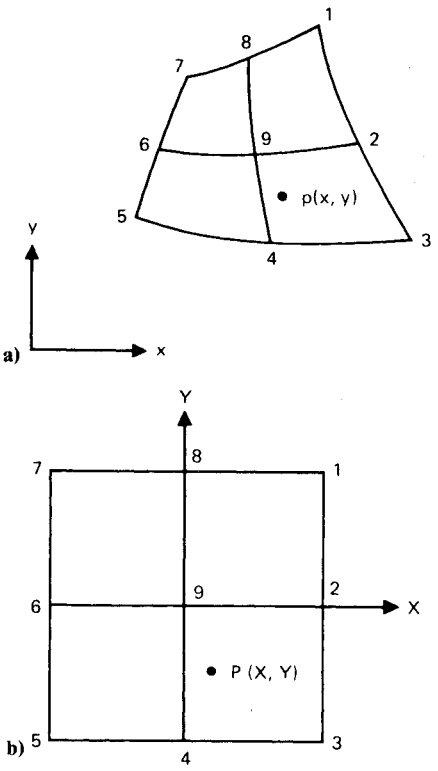

Fig. 1 Transformation of nine-point element: a) *x-y* (physical) plane; b) *X-Y* (computational) plane.

Presented as Paper 79-0012 at the AIAA 17th Aerospace Sciences Meeting New Orleans, La., Jan. 15-17, 1979; submitted Feb. 6, 1979; revision received Aug. 1, 1979.

Index categories: Transonic Flow; Computational Methods.

*Research Scientist, McDonnell Douglas Research Laboratories. Member AIAA.

†Consultant, McDonnell Douglas Research Laboratories; Assistant Professor, Sibley School of Mechanical and Aerospace Engineering, Cornell University, Ithaca, New York. Member AIAA.

Coordinate Transformation

Finite-difference methods are most conveniently and accurately applied in domains that are rectangular and subdivided by a uniform mesh. Therefore, in order to treat an arbitrary geometry, a coordinate transformation is required to transform the (usually) nonuniform physical grid to a uniform computational grid. A convenient method is to establish local coordinate transformations using shape functions that are common in finite-element analyses.[8] A nine-point isoparametric element will be used here. Within this element, the coordinates x and y of an arbitrary point p in the physical plane [see Fig. 1a] are related to the coordinates X and Y in the computational plane [see Fig. 1b] by

$$x=\psi^T x_i \tag{1}$$

$$y=\psi^T y_i \tag{2}$$

where ψ^T is the transpose of the column vector of the element shape functions, ψ, which is given by

$$\psi=\frac{1}{4}\begin{Bmatrix} XY(X+1)(Y+1) \\ -2X(X+1)(Y+1)(Y-1) \\ XY(X+1)(Y-1) \\ -2Y(X+1)(X-1)(Y-1) \\ XY(X-1)(Y-1) \\ -2X(X-1)(Y+1)(Y-1) \\ XY(X-1)(Y+1) \\ -2Y(X+1)(X-1)(Y+1) \\ 4(X+1)(X-1)(Y+1)(Y-1) \end{Bmatrix} \tag{3}$$

$$-\le X\le 1;-1\le Y\le 1$$

and the transposes of the column vectors of the mesh coordinate x and y are given by

$$x_i^T=[x_1,x_2,x_3,\ldots,x_9] \tag{4}$$

$$y_i^T=[y_1,y_2,y_3,\ldots,y_9] \tag{5}$$

where (x_1,y_1) $(x_2,y_2)\ldots$, and (x_9,y_9) are the coordinates of points 1, 2, . . ., and 9 in the physical plane, respectively (see Fig. 1). Similarly, the potential function ϕ within the element can be expressed as

$$\phi=\psi^T\phi_i \tag{6}$$

$$\phi_i^T=[\phi_1,\phi_2,\ldots,\phi_9] \tag{7}$$

Under a general coordinate transformation from (x,y) to (X,Y), the following results can be verified by application of the chain rule. Let

$$J=\begin{Bmatrix} x_X & x_Y \\ y_X & y_Y \end{Bmatrix} \tag{8}$$

represent the Jacobian matrix of the transformation. Then

$$J^{-1}=\frac{1}{D}\begin{Bmatrix} y_Y & -x_Y \\ -y_X & x_X \end{Bmatrix} \tag{9}$$

where

$$D=x_X y_Y-x_Y y_X \tag{10}$$

is the determinant of J. The velocities transform as

$$\begin{Bmatrix}\phi_x\\ \phi_y\end{Bmatrix}=(J^T)^{-1}\begin{Bmatrix}\phi_X\\ \phi_Y\end{Bmatrix} \tag{11}$$

It is frequently useful to express the velocity vector in terms of its contravariant components U and V in the transformed coordinate system

$$\begin{Bmatrix}U\\ V\end{Bmatrix}=J^{-1}\begin{Bmatrix}\phi_x\\ \phi_y\end{Bmatrix}=(J^TJ)^{-1}\begin{Bmatrix}\phi_Y\\ \phi_X\end{Bmatrix} \tag{12}$$

The second derivatives transform according to

$$\begin{Bmatrix}\phi_{xx}\\ \phi_{yy}\\ \phi_{xy}\end{Bmatrix}=-BCA\begin{Bmatrix}\phi_X\\ \phi_Y\end{Bmatrix}+B\begin{Bmatrix}\phi_{XX}\\ \phi_{YY}\\ \phi_{XY}\end{Bmatrix} \tag{13}$$

where

$$A=(J^T)^{-1}=\begin{bmatrix} x_X & y_X \\ x_Y & y_Y \end{bmatrix}^{-1} \tag{14}$$

$$B=\begin{bmatrix} x_X^2 & y_X^2 & 2x_Xy_X \\ x_Y^2 & y_Y^2 & 2x_Yy_Y \\ x_Xx_Y & y_Xy_Y & (x_Xy_Y+x_Yy_X) \end{bmatrix}^{-1} \tag{15}$$

$$C=\begin{bmatrix} x_{XX} & y_{XX} \\ x_{YY} & y_{YY} \\ x_{XY} & y_{XY} \end{bmatrix} \tag{16}$$

An explicit form of the matrix B is given in the Appendix.

Difference Equation

The full-potential equation to be solved is given as

$$(a^2-u^2)\phi_{xx}+(a^2-v^2)\phi_{yy}-2uv\phi_{xy}+a^2(v/y)=0 \tag{17}$$

where x and y are the axial and radial coordinates, respectively, and u and v are the x and y components of the flow velocity. The local speed of sound a is determined from the energy equation

$$a^2=a_0^2-(\gamma-1)(u^2+v^2)/2 \tag{18}$$

where γ is the ratio of specific heats for the assumed calorically perfect gas and a_0 is the stagnation speed of sound. On the axis, $y=0$, Eq. (17) becomes

$$(a^2-u^2)\phi_{xx}+2a^2\phi_{yy}=0 \tag{19}$$

Through the application of Eqs. (11) and (13), Eqs. (17) and (19), written in the Cartesian coordinates, can be rewritten in the computational coordinates X and Y. As mentioned previously, the mesh spacing in the X and Y coordinates is uniform; therefore, a simple finite-difference representation of the equations can be constructed. As suggested by Murman and Cole,[1] central differencing is used at mesh points where

the flow is locally subsonic. Applying Eqs. (1, 2, and 6) at the center of the element, i.e., point 9 (Fig. 1), the following central-difference expressions of coefficients $x_X, y_X, \phi_X, \ldots$ hold (setting $X=Y=0$ after differentiating ψ with respect to either X or Y):

$$x_X = \tfrac{1}{2}(x_2 - x_6) \tag{20a}$$

$$y_X = \tfrac{1}{2}(y_2 - y_6) \tag{20b}$$

$$\phi_X = \tfrac{1}{2}(\phi_2 - \phi_6) \tag{20c}$$

$$x_Y = \tfrac{1}{2}(x_8 - x_4) \tag{20d}$$

$$x_{XX} = x_2 - 2x_9 + x_6 \tag{20e}$$

$$x_{YY} = x_8 - 2x_9 + x_4 \tag{20f}$$

$$x_{XY} = \tfrac{1}{4}(x_1 - x_3 + x_5 - x_7) \tag{20g}$$

In order to stabilize the scheme in supersonic zones, a directional bias must be incorporated. For this purpose, it is convenient to rewrite Eq. (17) in coordinates aligned with the local flow direction s as

$$(a^2 - q^2)\phi_{ss} + a^2(\nabla^2\phi - \phi_{ss}) + a^2 v/y = 0 \tag{21}$$

where

$$q^2 = u^2 + v^2 \tag{22}$$

$$\phi_{ss} = 1/q^2(u^2\phi_{xx} + v^2\phi_{yy} + 2uv\phi_{xy}) \tag{23}$$

and

$$\nabla^2\phi = \phi_{xx} + \phi_{yy} \tag{24}$$

Substituting Eqs. (11) and (13) into Eqs. (23) and (24) gives

$$\phi_{ss} = 1/q^2(p_1\phi_{XX} + p_2\phi_{YY} + p_3\phi_{XY} - p_4\phi_X - p_5\phi_Y) \tag{25}$$

and

$$\nabla^2\phi = (h_1\phi_{XX} + h_2\phi_{YY} + h_3\phi_{XY} - h_4\phi_X - h_5\phi_Y) \tag{26}$$

where

$$\begin{Bmatrix} p_1 \\ p_2 \\ p_3 \end{Bmatrix} = \boldsymbol{B}^T \begin{Bmatrix} u^2 \\ v^2 \\ 2uv \end{Bmatrix} \tag{27}$$

$$\begin{Bmatrix} p_4 \\ p_5 \end{Bmatrix} = (\boldsymbol{BCA})^T \begin{Bmatrix} u^2 \\ v^2 \\ 2uv \end{Bmatrix} \tag{28}$$

$$\begin{Bmatrix} h_1 \\ h_2 \\ h_3 \end{Bmatrix} = \boldsymbol{B}^T \begin{Bmatrix} 1 \\ 1 \\ 0 \end{Bmatrix} \tag{29}$$

and

$$\begin{Bmatrix} h_4 \\ h_5 \end{Bmatrix} = (\boldsymbol{BCA})^T \begin{Bmatrix} 1 \\ 1 \\ 0 \end{Bmatrix} \tag{30}$$

An artificial viscosity is added in a form chosen to approximate the effect of upwind differencing the contributions to ϕ_{ss} in the first term of Eq. (21). This numerical viscosity emulates the rotated differencing scheme of Jameson,[2] but is added in conservation form, even though the equation itself is written in its nondivergence form. The terms added to Eq. (21) are given by[7]

$$H = (\mu f)_X + (\mu g)_Y \tag{31}$$

where

$$\mu = \max(0, 1 - (a^2/q^2)) \tag{32}$$

$$f = s(\Delta X)(p_1\phi_{XX} + p_3\phi_{XY}) \tag{33a}$$

$$g = t(\Delta Y)(p_2\phi_{YY} + p_3\phi_{XY}) \tag{33b}$$

$$s = \begin{cases} 1, \text{ if } U > 0 \\ -1, \text{ if } U < 0 \end{cases} \tag{34a}$$

$$t = \begin{cases} 1, \text{ if } V > 0 \\ -1, \text{ if } V < 0 \end{cases} \tag{34b}$$

For a comparison, a nonconservative scheme was also coded. For this scheme, the artificial viscosity term was expressed as

$$\begin{aligned} H = \mu\{ & p_1[(\phi_{XX})_{\text{U.W.}} - (\phi_{XX})_{\text{C.D.}}] \\ & + p_2[(\phi_{YY})_{\text{U.W.}} - (\phi_{YY})_{\text{C.D.}}] \\ & + p_3[(\phi_{XY})_{\text{U.W.}} - (\phi_{XY})_{\text{C.D.}}]\} \end{aligned} \tag{35}$$

where subscripts U.W. and C.D. represent upwind and central differencing, respectively. For example, if $\Delta X = 1$ [consistent with Eq. (3)],

$$(\phi_{XX})_{\text{U.W.}} = \phi_{i-2s} - 2\phi_{i-s} + \phi_i \tag{36}$$

$$(\phi_{XY})_{\text{U.W.}} = st/2(\phi_{i,j} + \phi_{i-s,j-t} - \phi_{i,j-t} - \phi_{i-s,j}) \tag{37}$$

It is important to note the essential difference between the quasiconservative and nonconservative formulations. The inviscid solution will not, in general, satisfy the conservation law of mass flux if discontinuities are present when the equation is differenced in nonconservative form. In the quasiconservative formulation, although the equation is not in the conservative form, the artificial viscosity term is added in the conservative form. This formulation generally yields results in good agreement with the fully conservative formulation[9,10] which must compute the density (a fractional power) at each mesh point in each iteration. However, the nonconservative formulation often provides results in better agreement with experiment, because the mass artificially added at a shock simulates the displacement thickening of the boundary layer caused by the shock-wave, boundary-layer interaction, which is neglected in the inviscid calculation.

The difference equations resulting from the preceding formulation are highly implicit; care must be taken to insure that the relaxation scheme used to solve them corresponds to a convergent process. As suggested by Jameson[2] and Caughey and Jameson,[4,7] it is useful to regard the relaxation scheme as a discrete approximation to a time-dependent process with the iteration steps corresponding to increments in an artificial time. Closely following the pattern of mixing old and updated values of the potential function, ϕ and ϕ^+ in approximating ϕ_{XX}, ϕ_{YY}, ϕ_{XY}, ϕ_X, and ϕ_Y as suggested by Jameson,[2]

substituting Eqs. (25) and (26) into Eq. (21), and adding the artificial viscosity term H, the following relaxation equations are constructed. Let i and j represent the indices of the mesh points in the X and Y directions, respectively. For a line relaxation scheme which solves the equations along lines of $X=$ const, the correction $C_{i,j} = \phi_{i,+j} - \phi_{i,j}$ to be added to the potential at each point, is determined by solving

$$\alpha_1(C_{i,j}-C_{i,j-1})+\alpha_2(C_{i,j}-C_{i,j+1}) +\alpha_3(C_{i,j}-C_{i-s,j})+\alpha_4 C_{i,j}=R \tag{38}$$

where R is the residual of Eqs. (21) or (17) evaluated with values of the potential from previous iteration, and

$$\alpha_1=a^2h_2-p_2+\mu(3p_2+stp_3)+\omega_s V(sU+tV)(t+1)/2D^2 \tag{39}$$

$$\alpha_2=a^2h_2-p_2+\mu p_2+\omega_s V(sU+tV)(t-1)/2D^2 \tag{40}$$

$$\alpha_3=a^2h_1-p_1+\mu(3p_1+stp_3)+\omega_s sU(sU+tV)/D^2 \tag{41}$$

$$\alpha_4=(2/\omega_r-1)(a^2h_1-p_1)\max(0,a^2-q^2)/(a^2-q^2) \tag{42}$$

Here ω_r is a subsonic overrelaxation factor chosen between 1 and 2. The ω_s factor governs the amount of the ϕ_{st} term added to the equivalent time-dependent equations governing the relaxation process; larger values lead to a more stable iteration, but slower convergence. In general, ω_s terms are needed only in the finest mesh and for high subsonic flow cases.

The coefficients given in Eqs. (39-42) are consistent with the coefficients used to compute the residual involving ϕ_{ss} and $\nabla^2\phi$ in Eqs. (25) and (26). We will refer to these coefficients as consistent coefficients. Because of the necessary matrix manipulation in this procedure, it usually requires additional computing time since the coefficients are computed at each mesh point in each iteration.

An alternative method, aimed at improving computing efficiency, is to solve for ϕ_{xx}, ϕ_{yy}, and ϕ_{xy} algebraically from Eq. (13), and then compute the residual using Eq. (17). In the process of constructing the relaxation scheme ϕ_{ss} and $\nabla^2\phi$ are approximated by their principal parts, as suggested by Caughey and Jameson[7]

$$\phi_{ss} \doteq \frac{1}{D^2q^2}(U^2\phi_{XX}+2UV\phi_{XY}+V^2\phi_{YY}) \tag{43}$$

$$\nabla^2\phi = 1/D(U_X+V_Y) \doteq B_{11}\phi_{XX}+2B_{12}\phi_{XY}+B_{22}\phi_{YY} \tag{44}$$

where B_{11}, B_{12}, B_{22} are the elements of matrix $(J^TJ)^{-1}$.

The corresponding coefficients of the relaxation equation thus obtained are given by

$$\alpha_1=a^2B_{22}-V^2/D^2+\mu(3V^2+2stUV)/D^2 +\omega_s V(sU+tV)(t+1)/2D^2 \tag{45}$$

$$\alpha_2=a^2B_{22}-V_2/D^2+\mu V^2/D^2+\omega_s V(sU+tV)(t-1)/2D^2 \tag{46}$$

$$\alpha_3=a^2B_{11}-U^2/D^2+\mu(3U^2+2stUV)/D^2 +\omega_s sU(sU+tV)/D^2 \tag{47}$$

$$\alpha_4=(2/\omega_r-1)(a^2B_{11}-U^2)\max(0,a^2-q^2)/(a^2-q^2) \tag{48}$$

These coefficients differ, in no essential way, from those given in Ref. 7, and are simpler in their form than the consistent coefficients, but fail to provide convergent solutions for some extreme geometry cases. We will refer to these coefficients as principal coefficients. Although the ϕ_{ss} and $\nabla^2\phi$ terms in Eqs. (43) and (44) are not exactly consistent with the ϕ_{ss} and $\nabla^2\phi$ terms in Eqs. (23) and (24), used to compute the residual, the relaxation equations still converge well to the solution as long as the truncated terms in Eqs. (43) and (44) are small compared with the principal parts. This is true for most of the regular geometries considered here.

Generation of Grid Network

As demonstrated in Ref. 7, one advantage of the previous approach in performing the local coordinate transformation is that the treatment of body boundary conditions becomes extremely simple, if the coordinate system is boundary-conforming. For the flowfield about a nacelle inlet with a center hub, two of the coordinate lines can be arranged to coincide with the lip and center hub contours, respectively. There are many possibilities of generating grid points in this manner; a convenient method is to follow a nearly conformal mapping procedure. Let $z=x+iy$, and $Z=X+iY$ be complex variables where real and imaginary parts represent the axial and radial coordinates in the physical and the computational variables, respectively, with the physical plane scaled so that the outer radius of the cowl lip is approximately equal to π. The geometry is first unwrapped about the cowl lip and hub singularities using the following conformal transformation[11]:

$$z=-\bar{\alpha}\cosh^2 Z-\ell n(\cosh^2 Z) \tag{49}$$

The parameter $\bar{\alpha}$ is determined by

$$\bar{\alpha}+\ell n\bar{\alpha}=-\alpha \tag{50}$$

where $\alpha-1$ is the axial separation of the singular points about which the hub and lip surfaces are unwrapped. After shear transformations to reduce the lip and hub surfaces to coordinate lines, a final rectangular domain is obtained where the

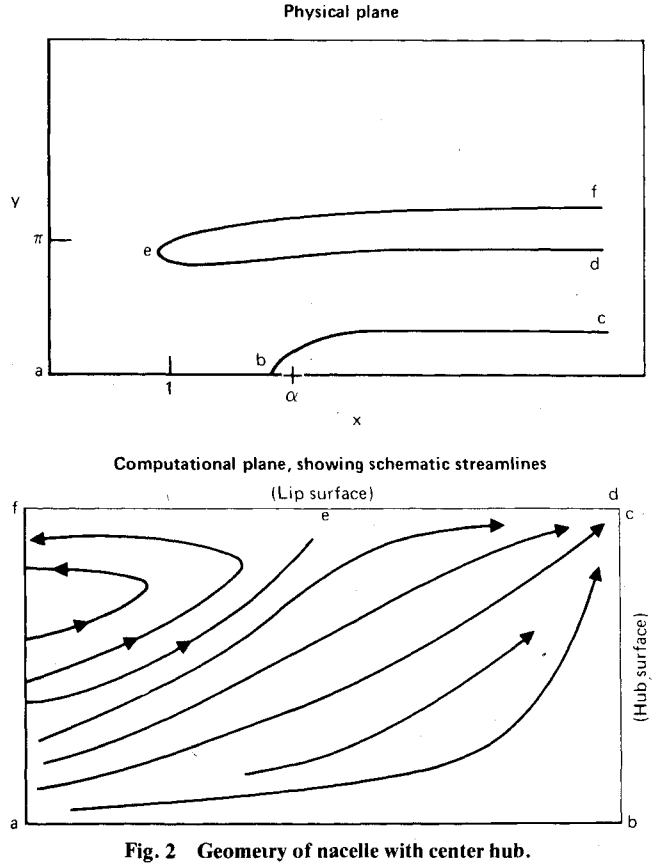

Fig. 2 Geometry of nacelle with center hub.

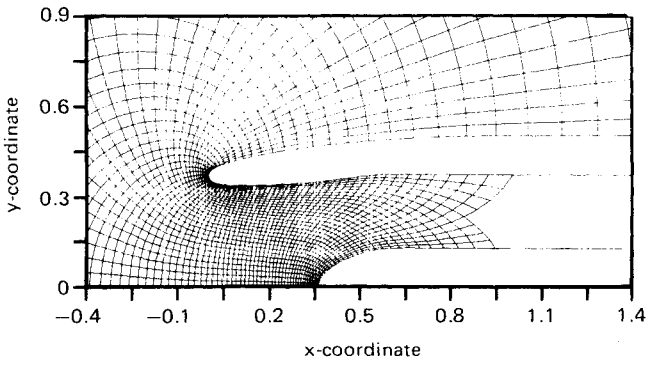

Fig. 3 DC-8 engine inlet contour and coordinate grid.

upper edge represents the lip surface and the right edge represents the hub surface. The physical and final computational planes are illustrated in Fig. 2. This sequence of transformations automatically produces a finer mesh in the neighborhood of the cowl lip and hub singularities as shown in Fig. 3 for a typical cowl-hub geometry.

Although the conformal mapping procedure is straightforward to apply, in some extreme geometries, the mesh may be ill-behaved near singularities and need special treatment. For nacelle geometries without centerbodies, the previous conformal transformation can be used to generate mesh points outside the nacelle and near the vicinity of the lip nose, and an interpolation method can be used to generate mesh points inside the nacelle. This piecewise approach to generate mesh is possible because the present method requires only local knowledge of the coordinate transformation and knowledge of the global nature of the mapping functions is not essential.

Boundary Conditions

In order to eliminate the singularity in the velocity potential at infinity outside the nacelle, the potential function ϕ is expressed as

$$\phi = U_\infty x + G \tag{51}$$

where U_∞ is the freestream velocity and the reduced potential G is determined numerically.

For nonzero freestream speed cases, the freestream speed is set equal to 1, and for zero freestream speed cases, the freestream sonic speed is set equal to 1. Examples of cases of both types are presented in the subsequent sections. With Eq. (51), the boundary condition at infinity outside the nacelle is simply $G=0$.

The boundary condition at downstream infinity inside the nacelle (or at the compressor face) is specified to be a prescribed uniform axial velocity u_K. The isentropic mass flux relation

$$\frac{u_K}{U_\infty} = \frac{A_{hl}}{A_{cf}} Q\left\{1-(\gamma-1)M_\infty^2\left[\left(\frac{u_K}{U_\infty}\right)^2-1\right]/2\right\}^{-(1/\gamma-1)} \tag{52}$$

is used to determine u_K in terms of $Q = A_0/A_{hl}$, the conventional mass flux ratio where A_0 is the cross-sectional area of the captured stream tube at upstream infinity; A_{hl} is the area of the inlet based on the hilite radius; A_{cf} is the cross-sectional area at downstream infinity inside the nacelle; and M_∞ is the freestream Mach number.

For the zero freestream velocity case, the capture area and mass flow ratio are infinite and u_K is either specified or determined from the average Mach number specified at some internal station.

The surface boundary condition is implemented by imposing a zero normal velocity component. This condition is introduced by using the surface boundary condition to determine either the solution at surface points or at dummy points inside the boundary. In the latter case, the equation is solved at points on the boundary using the same formulas used at internal field points. Along the lip surface, the boundary condition is $V=0$ or

$$v/u = y_X/x_X \tag{53}$$

Along the hub surface, the boundary condition is $U=0$ or

$$v/u = y_Y/x_Y \tag{54}$$

If the surface boundary condition is applied to determine the solution at dummy points inside the boundary, the central-differencing formulas given in Eqs. (20a) and (20d) are used. If the surface boundary condition is used to determine the solution at surface points, central differencing is used along the boundary and one-sided differencing is used in the surface normal direction. For example, if in Fig. 1 the lip surface lies along the 7-8-1 face of the cell, the value of potential function at point 8 is to be determined. After differentiating ψ, Eq. (3), with respect to either X or Y, and then setting $X=0$ and $Y=1$, Eqs. (1, 2, and 6) yield

$$x_X = \tfrac{1}{2}(x_1 - x_7) \tag{55a}$$

$$y_X = \tfrac{1}{2}(y_1 - y_7) \tag{55b}$$

$$x_Y = \tfrac{1}{2}(3x_8 - 4x_9 + x_4) \tag{55c}$$

$$y_Y = \tfrac{1}{2}(3y_8 - 4y_9 + y_4) \tag{55d}$$

$$\phi_X = \tfrac{1}{2}(\phi_1 - \phi_7) \tag{55e}$$

$$\phi_Y = \tfrac{1}{2}(3\phi_8 - 4\phi_9 + \phi_4) \tag{55f}$$

Using Eqs. (55a-55d), the Jacobian coefficients x_X, y_X, x_Y, and y_Y can be computed at point 8, and matrix J is obtained. Applying Eq. (53) and substituting Eqs. (55a) and (55f) into Eq. (11), the value of the potential function at point 8, ϕ_8 can be determined if ϕ_1, ϕ_7, ϕ_9, and ϕ_4 are known. Similarly, the boundary condition along the hub surface, Eq. (54), can be applied to determine the value of the potential function at the hub surface.

The expressions for the first derivatives given in Eqs. (20) and (55) have the same order of accuracy; therefore, applications of the boundary condition to determine the solution at the surface points or at the dummy points inside the boundary should give nearly identical results. This fact was confirmed in the calculations.

Computational Considerations

The line-relaxation scheme described previously is applied to solve for the flowfields about nacelles with and without centerbodies. A computer program has been written with the capability of solving the implicit equation along lines of constant X or Y. The directional property of the supersonic flows must be considered carefully to insure stability of the iterative procedures. For the X-line scheme, the flowfield is swept from the lip leading edge toward the downstream, first for the inside of the nacelle, then for the outside. For the Y-line scheme, the field is swept from the axis of symmetry to the lip surface. Since the convergence rate of the iteration decreases and the computing cost increases as the mesh spacing goes to zero, it is effective first to compute the solution on a coarse mesh, and then successively compute the solutions on refined meshes with the solution on the previous mesh as an initial estimate. All of the calculations presented here use a sequence of three meshes.

The convergence rate also depends on the mass flow ratio. For large values of u_K, the solution depends strongly on the boundary condition at the compressor face and this in-

formation propagates slowly into flowfield, particularly when using the X-line scheme. For zero freestream speed cases, this effect is pronounced and the convergence rate is exceptionally slow; therefore, accelerated schemes seem to be desirable. The extrapolated-relaxation scheme described by Caughey and Jameson[4] was incorporated in the computer program to improve the convergence of solutions.

Although the formulations based on the nine-point element scheme described herein and the overlapping element scheme suggested by Caughey and Jameson[7] are different, their formal accuracies are of the same order. The second derivatives in these two approaches are computed differently. In the nine-point element schemes, the governing equation in Cartesian coordinates is applied directly, while in the overlapping element scheme, a special quasilinear equation written in contravariant velocity components is used. Both formulations have been programmed. In the computer program, only the solution array and the Cartesian coordinates of each mesh point are stored; therefore, the transformation matrix is computed at each mesh point in each iteration. In the nine-point element scheme, if the consistent relaxation coefficients are used and the matrix manipulation is performed, more time is required to compute the residual than the principal relaxation coefficients. A single relaxation sweep of the entire flowfield on a 128 × 32 mesh requires 0.940 s on the Cyber 175 for the former scheme and 0.557 s for the latter scheme. If the overlapping element scheme which applies principal coefficients is used, the same sweep requires 0.702 s. Although using consistent relaxation coefficients takes longer in computing time, it gives better results if highly distorted elements must be used. In the overlapping element scheme, the transformation matrices must be computed for three different overlapping elements at each mesh point, while in the nine-point element scheme, only one transformation matrix must be computed.

The computing efficiency of the preceding schemes can also be seen by comparing the number of operations, multiplication, division, addition, and subtraction needed to compute the residual in the program. In the nine-point element schemes, these numbers are roughly 240 and 160, using the consistent and principal relaxation coefficients, respectively. In the overlapping element scheme, this number is 160. For a three-dimensional problem, it would be expensive to use consistent relaxation coefficients in the equivalent nine-point element scheme, since the number of operations needed, including inverting a 6 × 6 matrix, to compute the residual is ~1700. Using the principal relaxation coefficients in either the equivalent nine-point element scheme or the overlapping element scheme, however, requires ~400 operations. In general, by using principal relaxation coefficients, the nine-point element scheme provides accurate and fast solutions, at least as good as the overlapping element scheme; by using the consistent relaxation coefficients, the nine-point element scheme has the additional feature of handling more highly distorted element shapes.

Numerical Results

Results of calculations performed using the analysis just described are presented and compared with experimental data. Two types of experimental data will be used. The first type deals with a research cowl without the center hub designed and tested by the Douglas Aircraft Company.[13] The shape of the cowl and a representative coordinate grid are shown in Fig. 4, and the measured and calculated pressure distributions on the outside surface of the cowl are presented in Figs. 5-7. The three cases are for the same mass flow ratio of 0.700 and for the freestream Mach numbers of 0.700, 0.851, and 0.900, respectively. The nonconservative numerical solutions shown are those obtained by Caughey and Jameson.[4] With the present method, both nonconservative and quasiconservative numerical solutions were obtained on a 128 × 32 grid and compared with those of

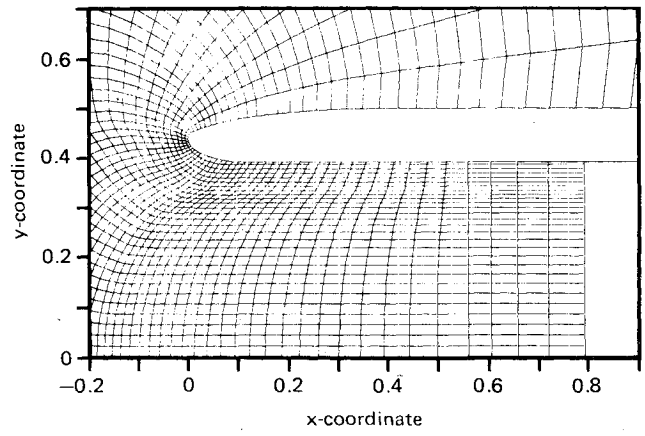

Fig. 4 Douglas research cowl contour and coordinate grid.

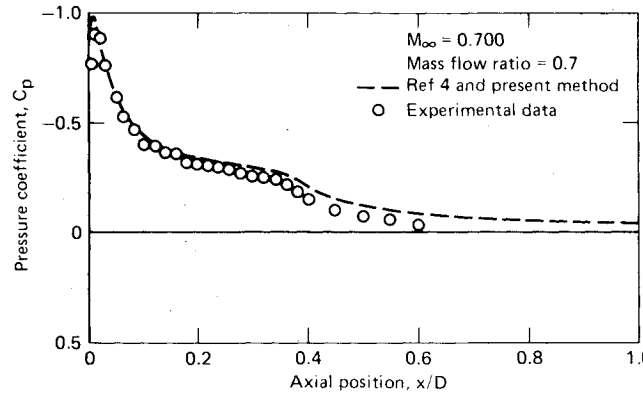

Fig. 5 Pressure distribution on the outer surface of the cowl lip ($M_\infty = 0.700$).

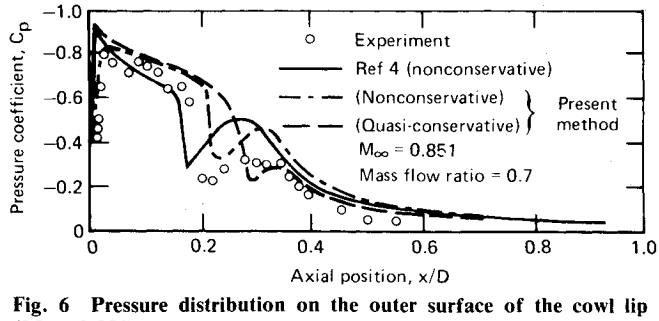

Fig. 6 Pressure distribution on the outer surface of the cowl lip ($M_\infty = 0.851$).

Caughey and Jameson as well as with the experiment. The accelerated scheme improves the convergence rates on all meshes and is particularly effective on the coarse ones. On the 128 × 32 mesh, the number of iterations required to converge the maximum residual to less than 10^{-6}, normalized by the square of stagnation speed of sound, is about 230 using principal relaxation coefficients, and the total CPU time required for a complete run is 3.5 min. The damping term with $\omega_s > 0.4$ must be added to stabilize the quasiconservative solution for the case $M_\infty = 0.900$. Figures 5-7 show that the nonconservative solutions give better prediction of the shock location, and the quasiconservative solutions give better prediction of the shock strength. This phenomenon has also been observed in transonic airfoil calculations.[10,12] There is a slight discrepancy between the nonconservative solutions obtained by the present method and those obtained by Caughey and Jameson[4] using the globally transformed governing equation. Several reasons might account for this discrepancy. The shock location is a rather sensitive feature of

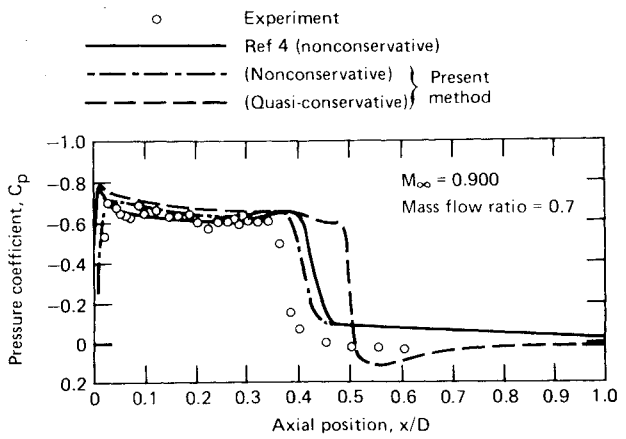

Fig. 7 Pressure distribution on the outer surface of the cowl lip ($M_\infty = 0.900$).

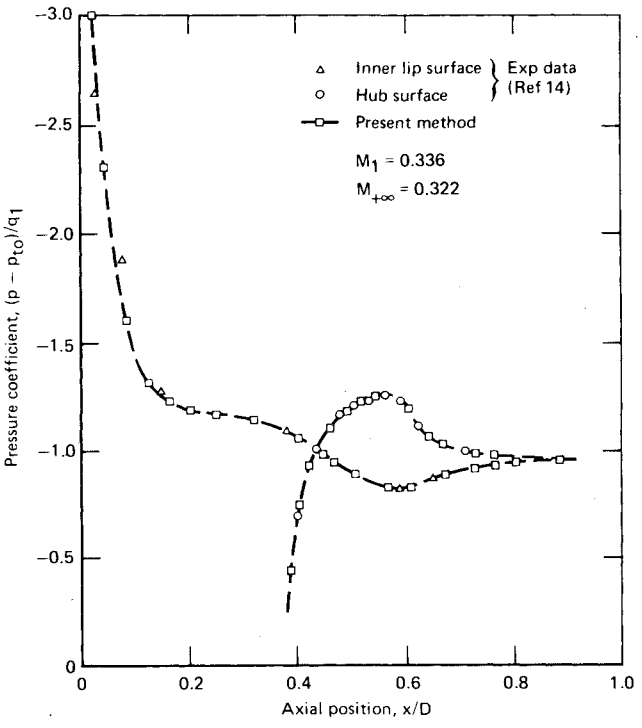

Fig. 8 Pressure distribution on DC-8 engine inlet for $M_1 = 0.336$ and $M_{+\infty} = 0.322$.

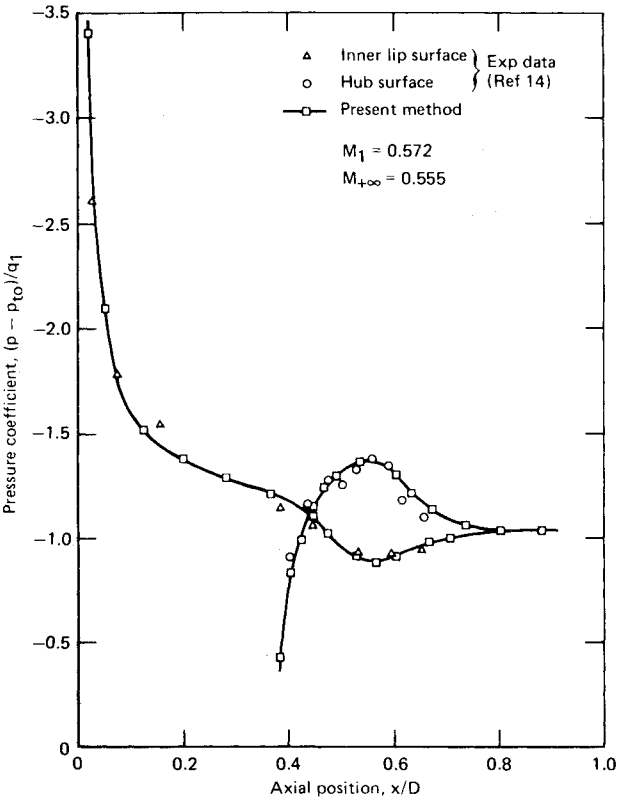

Fig. 9 Pressure distribution on DC-8 engine inlet for $M_1 = 0.572$ and $M_{+\infty} = 0.555$.

the flow. If the local meshes are not identical in the two computations, the solutions may differ slightly. (The discrepancy in shock location is of the same order as the mesh spacing in the region of interest.) Also, the truncation error in the present scheme would be expected to be larger, since the metric of the transformation is calculated numerically. To help compensate for this error, a higher-order element may be needed.

The second type of experimental data was obtained from a noise suppression study conducted at nearly zero freestream speed and employing modified DC-8 engine inlets with regular and enlarged centerbodies.[14] In the present calculations, the freestream Mach number was identically zero, and the Mach number at the compressor face, $M_{+\infty}$, was determined from the experimental data, i.e., from the asymptotic value of C_p

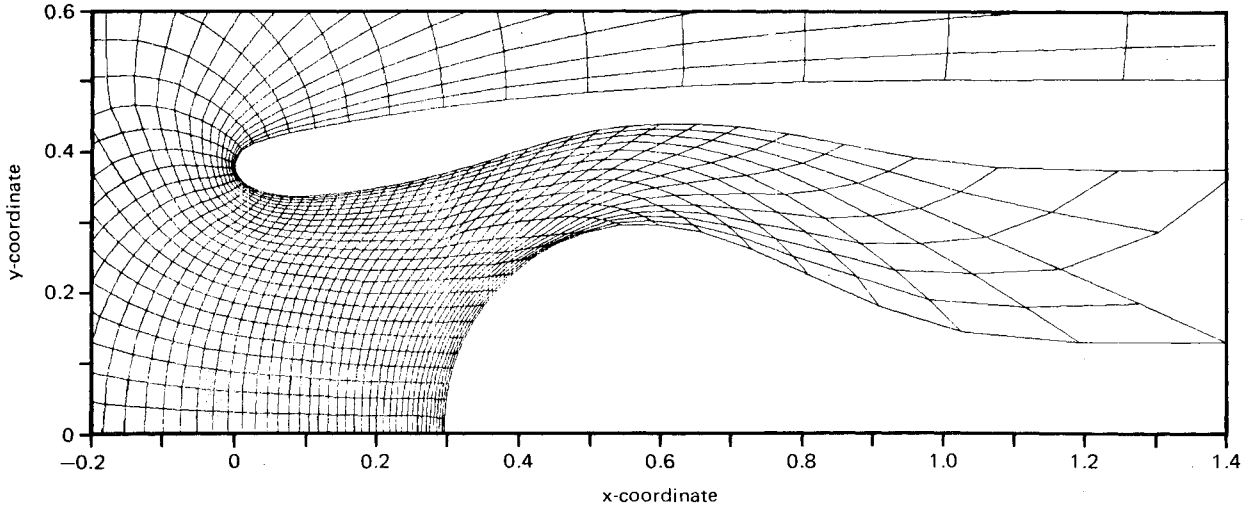

Fig. 10 Contour and coordinate grid of a modified DC-8 engine inlet (intermediate mesh).

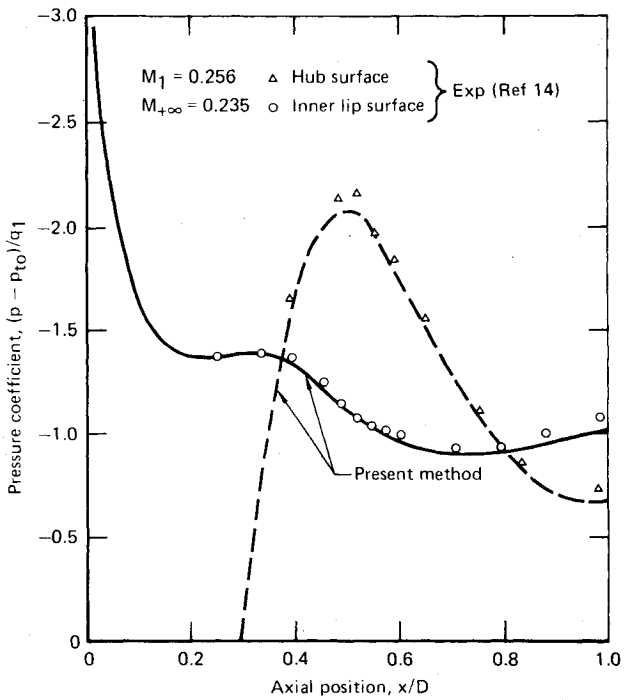

Fig. 11 Pressure distribution on a modified DC-8 engine inlet with enlarged hub.

at downstream infinity inside the nacelle. Figures 8 and 9 present results for a modified DC-8 engine inlet with a regular centerbody calculated on a 128 × 48 mesh. The inlet shape and grid are shown in Fig. 3. The pressure coefficient on the cowl lip and hub surfaces, normalized by the dynamic pressure at the cowl throat, is presented and compared with test data. M_1 is the average Mach number at the cowl throat, estimated from the experimental data. Figure 11 shows results for a modified DC-8 engine inlet with an enlarged centerbody, the shape and a representative coordinate grid of which are shown in Fig. 10. Although viscous effects in these cases are neglected, agreement between the numerical and experimental results is generally very good. On the 128 × 48 mesh, the number of iterations required to converge the maximum residual to less than 10^{-6} is about 400 using consistent relaxation coefficients, and the total CPU time required for a complete run is about 21 min. For this case, the solution did not converge well using the principal coefficients, and the accelerated scheme works exceptionally well on the finest mesh when the consistent coefficients are used.

Conclusion

A method is presented for calculating inviscid supercritical flowfields about axisymmetric inlet cowls with centerbodies using generalized coordinates. The method is shown to be fast and stable. Because of the use of boundary-conforming coordinates, the treatment of boundary conditions is extremely simple, and because of the use of local coordinate transformations, a global transformation of the governing equation is avoided. Both quasiconservative and nonconservative schemes are considered in the computations. The quasiconservative scheme generally provides a better presentation of the shock strength, while the nonconservative scheme provides a better prediction of the shock location. Numerical results for pressure distributions on the outside surface of nacelles corresponding to high-subsonic freestream speeds and for pressure distributions on the inside walls and along the center hub at high inlet mass flow rates and zero freestream speeds agree well with experiments.

Appendix

A useful alternative form of matrix $\boldsymbol{B}$ is:

$$\boldsymbol{B} = 1/D^2 \begin{bmatrix} y_Y^2 & y_X^2 & -2y_Y y_X \\ x_Y^2 & x_X^2 & -2x_Y x_X \\ -y_Y x_Y & -y_X x_X & (x_X y_Y + x_Y y_X) \end{bmatrix} \quad \text{(A1)}$$

where

$$D = x_X y_Y - x_Y y_X \quad \text{(A2)}$$

Acknowledgment

This work was supported by the McDonnell Douglas Corporation Independent Research and Development Program.

References

[1] Murman, E.M. and Cole, J.D., "Calculation of Plane Steady Transonic Flows," *AIAA Journal*, Vol. 9, Jan. 1971, pp. 114-121.

[2] Jameson, A., "Iterative Solution of Transonic Flows Over Airfoils and Wings, Including Flows at Mach 1," *Communications on Pure Applied Mathematics*, Vol. 27, 1974, pp. 283-309.

[3] Arlinger, B.G., "Calculation of Transonic Flow Around Axisymmetric Inlets," *AIAA Journal*, Vol. 13, Dec. 1975, pp. 1614-1621.

[4] Caughey, D.A. and Jameson, A., "Accelerated Iterative Calculations of Transonic Nacelle Flowfields," *AIAA Journal*, Vol. 15, Oct. 1977, pp. 1474-1480.

[5] Reyhner, T.A., "Cartesian Mesh Solution for Axisymmetric Transonic Potential Flow Around Inlets," *AIAA Journal*, Vol. 15, May 1977, pp. 624-631.

[6] Reyhner, T.A., "Transonic Potential Flow Around Axisymmetric Inlets and Bodies at Angle-of-Attack," *AIAA Journal*, Vol. 15, Sept. 1977, pp. 1299-1306.

[7] Caughey, D.A. and Jameson, A., "Numerical Calculation of Transonic Potential Flow About Wing-Body Combinations," *AIAA Journal*, Vol. 17, Feb. 1979, pp. 175-181.

[8] Zienkiewicz, O.C., *The Finite Element Method in Engineering Science*, McGraw-Hill, London, New York, 1971.

[9] Bauer, F. Garabedian, P., Korn, D., and Jameson, A., *Supercritical Wing Sections II, Lecture Notes in Economics and Mathematical Systems*, Vol. 108, Springer-Verlag, New York, 1975.

[10] Bauer, F. and Korn, D., "Computer Simulation of Transonic Flow Past Airfoils with Boundary Layer Correction," *AIAA 2nd Computational Fluid Dynamics Conference*, June 1975, pp. 184-189.

[11] Caughey, D.A., "A Systematic Procedure for Generating Useful Conformal Mappings," *International Journal for Numerical Methods in Engineering*, Vol. 12, Nov. 1978, pp. 1651-1657.

[12] Murman, E.M., "Analysis of Embedded Shock Waves Calculated by Relaxation Methods," *AIAA Journal*, Vol. 12, May 1974, pp. 626-633.

[13] Unpublished data, Douglas Aircraft Company, Long Beach, Calif.

[14] Marsh, A.H., Elias, I., Hoehne, J.C., and Frasca, R.L., "A Study of Turbofan-Engine Compressor-Noise-Suppression Techniques," NASA CR-1056, June 1968.